

Earth rotation parameter estimation from LLR and impact of non-tidal station loading

Vishwa Vijay Singh^{*1,2}, Liliane Biskupek¹, Jürgen Müller¹, and Mingyue Zhang¹

¹Institute of Geodesy (IfE), Leibniz University Hannover, Schneiderberg 50, 30167 Hannover, Germany

²Institute for Satellite Geodesy and Inertial Sensing, German Aerospace Center (DLR), Callinstraße 36, 30167 Hannover, Germany

31st December, 2021

Abstract

Lunar Laser Ranging (LLR) measures the distance between observatories on Earth and retro-reflectors on Moon since 1969. In this paper, we estimate the Earth Rotation Parameters (ERP; terrestrial pole offsets, x_p and y_p , and Earth rotation phase, ΔUT) using LLR data. We estimate the values of ΔUT , and the pole offsets separately. For the pole offsets, we estimate the values of x_p and y_p together and separately. Overall, the uncertainties of ERP from the new LLR data (after 2000.0) have significantly improved, staying less than 20 μs for ΔUT , less than 2.5 mas for x_p , and less than 3 mas for y_p for nights selected from subsets of the LLR time series which have 10 and 15 normal points obtained per night. Furthermore, we add the non-tidal loading effect provided by the International Mass Loading Service (IMLS), as observation level corrections of the LLR observatories in the analysis. This effect causes deformations of the Earth surface up to the centimetre level. Its addition in the Institute of Geodesy (IfE) LLR model, leads to a marginal improvement in the uncertainties ($3\text{-}\sigma$ values) of about 1% for both, ΔUT and the pole offsets.

Keywords— lunar laser ranging; non-tidal loading; Earth rotation parameters

1 Introduction

Lunar Laser Ranging (LLR) is the measurement of round trip travel times of short laser pulses between observatories on the Earth and retro-reflectors on the Moon. This has been possible since 1969, when the astronauts of Apollo 11 deployed the first retro-reflector on the lunar surface. Now there are five retro-reflectors on the Moon, and measurements have primarily been carried out from six observatories on the Earth that were or are capable to range to the Moon: the Côte d’Azur Observatory, France (OCA), the McDonald Laser Ranging Sta-

tion, USA (MLRS), the Apache Point Observatory Lunar Laser ranging Operation, USA (APOLLO), the Lure Observatory on Maui island, Hawaii, USA (LURE), the Matera Laser Ranging Observatory, Italy (MLRO) and the Geodetic Observatory Wettzell, Germany (WLRs). As the amount of signal loss of the laser pulse is enormous, it is necessary to collect single measurements for 5 to 15 minutes. Of these, a statistically secured mean value is computed, a so called normal point (NP). Details of the LLR measurement process can be found, for example, in Murphy [2013] and Müller et al. [2019]. LLR being the longest observation time series of all space geodetic techniques [Müller et al., 2019] allows the determination of a variety of parameters of the Earth–Moon dynamics, such as the mass of the Earth–Moon system, the lunar orbit and libration parameters [Williams et al., 2013; Pavlov et al., 2016], terrestrial and celestial reference frames and coordinates of observatories and reflectors [Müller et al., 2009; Hofmann et al., 2018] etc. Additionally, it leads to improvements in the solar system ephemerides [Kopeikin et al., 2008; Folkner et al., 2014; Pavlov et al., 2016], selenophysics [Murphy, 2013; Hofmann, 2017; Viswanathan et al., 2019], and gravitational physics [Williams et al., 2006; Müller et al., 2012; Hofmann and Müller, 2018; Zhang et al., 2020; Biskupek et al., 2021]. Furthermore, LLR can also be used to provide tests of Earth orientation parameters [Biskupek, 2015; Hofmann et al., 2018].

The terrestrial pole offsets (or, polar motion coordinates (PMC)), x_p and y_p , describe the change of the rotation axis in relation to the Earth’s surface. The Earth rotation phase ΔUT and the Length-of-Day (LOD) refer to the rotational motion of the Earth. All these parameters are summarised as Earth Rotation Parameter (ERP). Together with the celestial pole offsets, δX and δY , as corrections to the conventional precession–nutation model, they define the Earth Orientation Parameters (EOPs). The EOP values are combined from different space geodetic techniques [Bizouard et al., 2019], such as Very Long Baseline Interferometry (VLBI), Global Navigation Satellite System (GNSS), Satellite Laser Ranging (SLR) and Doppler Orbitography and Radiopositioning Integrated by Satellite (DORIS), and published^{1,2} by the Earth Orientation Centre (EOC) of the International Earth Rotation and Refer-

¹<http://www.iers.org/IERS/EN/DataProducts/EarthOrientationData/eop.html>

²<https://hpiers.obspm.fr/eop-pc/index.php?index=C04&lang=en>

*Corresponding author:
Vishwa Vijay Singh, email: singh@ife.uni-hannover.de

ence Systems Service (IERS). LLR products are not yet a part of the EOPs published by the IERS (as IERS EOP 14 C04 series). The Kalman Earth Orientation Filter (KEOF) COMB series, of Ratcliff and Gross [2020] exists as an alternative to the IERS C04 series. It is calculated from the data of LLR, SLR, VLBI and GNSS.

The EOPs obtained from LLR and other space geodetic techniques are different in their realisation. LLR is the only space geodetic technique which provides a dynamical realisation of the celestial reference system, [Zerhouni and Capitaine, 2009], whereas other space geodetic techniques provide a kinematic realisation of the celestial reference system. Additionally, ΔUT values can only be obtained from VLBI and LLR, making results from LLR useful in validating the results from VLBI.

In this study, we estimate the Earth rotation phase (ΔUT) and terrestrial pole offsets (x_p and y_p) using LLR data. Section 2 defines the data and methods of calculations used for the estimation of ΔUT (in section 3), and x_p and y_p (in section 4). In section 3 and section 4, we give the most recent results and discuss the accuracy of the ERPs, analyse the correlations of the estimated parameters with each other, and additionally study the effect of non-tidal loading (NTL) on the estimated values of x_p and y_p , and ΔUT . In section 5, we give the conclusions to this study.

2 Data and method

In Germany, from the early 80ies, the software package LUNAR (LUNar laser ranging Analysis softwaRe) has been developed to study the Earth-Moon system and to determine several related model parameters [Egger, 1985; Gleixner, 1986; Bauer, 1989; Müller, 1991]. The analysis model used in LUNAR is based on Einstein’s theory of relativity. It is fully relativistic and complete up to the first post-Newtonian ($1/c^2$) level. To take advantage of the high-precision NPs that can be obtained with an accuracy of several millimetres [Murphy, 2013], the LUNAR software was updated continuously [Biskupek, 2015; Hofmann, 2017]. A recent overview of LUNAR is given in Hofmann et al. [2018], a detailed description can be found in Müller et al. [2014]. The adjustment is done in a Gauss-Markov model (GMM) where, in the current version of LUNAR, up to 200 unknown parameters can be determined with their uncertainties.

2.1 LLR data

The distribution of LLR NPs has a big impact on the determination of various parameters. Non-uniform data distribution is one of the reasons for correlations between solution parameters [Williams et al., 2009]. From 2015, many NPs were measured using laser pulses of infra-red wavelength, due to which ranging near new and full Moon became possible [Chabé et al., 2020] for OCA and WLRs. This leads to a better coverage of the lunar orbit over the synodic month, i.e. the time span in which the Sun, the Earth, and the Moon return to a similar constellation again. With a better coverage of the lunar orbit, it is possible to perform a more uniform estimation of ERPs. Fig. 1 shows the temporal distribution of the measured NPs since 1970. In

the analysis, the three observatories McDonald, MLRS1, and MLRS2 are linked by local ties and analysed together, and are therefore listed in the figure as MLRS. OCA measurements with laser wavelength of $\lambda = 684.3\text{ nm}$ and $\lambda = 532\text{ nm}$ are listed in the figure as OCA green. As given in the legend of Fig. 1, more than 60% of the NPs were observed by OCA (40% with green and 21% with infra-red (IR) laser light). In the last years, only OCA and APOLLO provided regular NPs, and MLRO and WLRs only contributed a few NPs. For the year 2020, 84% of the NPs were measured by OCA in IR. Therefore, with this distribution of NPs, the overall analysis is dominated by the OCA NPs.

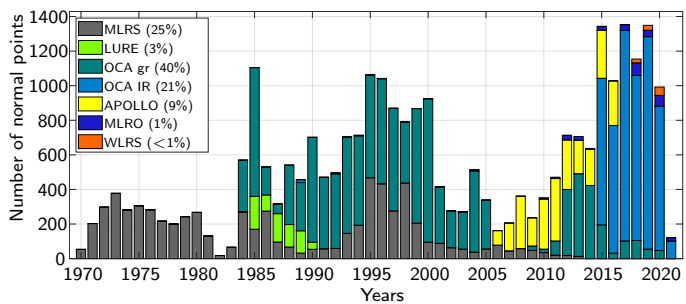


Figure 1: Distribution of the 28 093 normal points over the time span April 1970 - April 2021. In the legend the percentages of the contribution of the respective observatories are given. The three observatories McDonald, MLRS1 and MLRS2 are linked in the analysis and listed here as ‘MLRS’. OCA measurements with laser wavelength of $\lambda = 684.3\text{ nm}$ and $\lambda = 532\text{ nm}$ are listed as ‘OCA gr’.

The measured NPs serve as observations in the analysis. They are treated as uncorrelated for the stochastic model of the least squares adjustment and are weighted according to their measurement accuracies.

2.2 ERP a-priori data and estimation

In LUNAR, as a-priori ERP values, the KEOF COMB2019 series [Ratcliff and Gross, 2020] is used until 0h UTC 01.01.1983 and the IERS EOP 14C04 series is used from 0h UTC 02.01.1983 onward. The differences between KEOF COMB2019 and IERS 14 C04 series are of a few μs for the PMC and a few μs for ΔUT after January 1, 2000. Before 2000, these differences are up to a few ms for ΔUT and a few mas for the PMC. Further details about the differences between IERS 14 C04 series and the COMB series can be found in [Ratcliff and Gross, 2020]. This implementation of two different EOP time series within LUNAR is done as the COMB2019 series includes LLR data in its formation, and therefore fits the initial phase of the observations better. After 01.01.1983, the differences between the two series become smaller, and therefore we use the IERS 14 C04 to benefit from its shorter latency period.

As the rotation matrix between the Earth fixed International Terrestrial Reference System (ITRS) and the space fixed Geocentric Celestial Reference System (GCRS) includes the PMC and ΔUT in its calculation, these can be estimated from LLR analysis, as shown by Dickey et al. [1985]; Müller [1991]; Biskupek [2015]. The most recent results of ERP from LLR

have been discussed by Hofmann et al. [2018]. Biskupek [2015] gave the equations for the partial derivatives of ERP (used for the adjustment) and discussed the results of the different possible methods to obtain ERP from LUNAR (selecting time spans or specific nights for which ERP are adjusted) for 20 047 NPs (1970 - 2013), where the accuracy of ΔUT achieved was a maximum of 0.14 ms (70 day period of estimation), and the accuracy of the PMC was in the range of 30 - 90 mas for different combinations of observatories from which the PMC were estimated (x_p and y_p were estimated individually, due to high correlations with each other). Hofmann et al. [2018] discussed the results of estimation of the Earth rotation phase for 23 261 NPs (1970 - 2016), achieving an accuracy under 0.089 ms when estimating ΔUT from all observatories, and under 0.044 ms when estimating ΔUT from only OCA and APOLLO.

The ERP estimation from other techniques leads to better results than those from LLR, due to the availability of much more data and a better global coverage. The accuracies achieved from different space geodetic techniques are given in Table 1, where it can be seen that the best results of the PMC are from GNSS, primarily due to dense network of its stations. The sensitivities of the space geodetic techniques are different for various EOPs, and not all techniques can determine all parameters, for example, ΔUT values can only be obtained from VLBI and LLR.

Table 1: Accuracies of the ERPs obtained from different space geodetic techniques [Sciarretta et al., 2010; Schuh and Behrend, 2012; Capitaine, 2017; Zajdel et al., 2020].

Technique	Parameters	
	PMC	ΔUT
VLBI	50 - 80 μas	1 - 5 μs
SLR	10 - 30 μas	-
GPS	5 - 20 μas	-

Since 2015, IR NPs measurements are available from OCA. These enable a better coverage of the lunar orbit and obtain more NPs per night, leading to a better and more stable estimation of ERPs from LLR, which achieves higher accuracy compared to previous results. For ERPs determination from the LLR analysis, the whole dataset of NPs is pre-analysed. Here, different configurations can be taken into account, which also define the configuration in the analysis, thereby making it possible to vary the number of NPs per night and to estimate ERPs from the data of all observatories or only for a single observatory.

As shown in Fig. 1, the number of NPs measured per year has significantly risen over the past few years, implying that more NPs were recorded per night, and that they were recorded for more nights. Despite having more NPs per night over the past years, it is currently still difficult to estimate PMC and ΔUT together for one night and one observatory due to their high correlation with each other. Therefore, in the current study, either PMC (x_p and y_p individually, and together) or ΔUT were determined, where the other values were fixed to the a-priori EOP series. It is also difficult to determine ERPs with the coordinates and velocities of the observatories together for one night, therefore, the velocities of the observatories were

fixed to the ITRF2014 solution values^{3,4}.

The selection of nights was based on the observatory/observatories where the NPs were measured from (only from APOLLO, only from OCA, or from all observatories). We selected only subsets of nights in which at least 5, 10, and 15 NPs were measured. Table 2 gives details of the subsets which were created for this study, and the abbreviations we use to refer to these subsets.

Table 2: Details of the data subsets which were created for this study along with their time spans and abbreviations used for them.

Obs.*	NPs per night	No. of nights	Abbreviation used	Time span
APOLLO	5	261	Apollo05	04.06.2006
				-
	10	63	Apollo10	26.10.2016
				-
OCA	5	1320	OCA05	29.03.2008
				-
	10	714	OCA10	24.10.2016
				-
	15	355	OCA15	07.04.1984
				-
-	-	-	30.03.2021	
All	5	1975	All05	08.04.1984
				-
	10	914	All10	24.03.2021
				-
15	450	All15	29.09.1983	
			-	
-	-	-	19.01.2021	

*Observatory/Observatories

Preliminary studies showed that the accuracies of the ERPs determined in our LLR adjustment were too optimistic. Comparisons with other parameters led to the conclusion that a 3σ -accuracy is a realistic specification for the accuracies in our

³as APOLLO observatory is not included in the ITRF2014 solution, we used the velocity for White Sands GNSS observatory (DOMES number: 49884S001) as the replacement

⁴https://itrf.ign.fr/ITRF_solutions/2014/more_ITRF2014.php

LLR analysis. For this reason, all accuracies for ERPs are given as 3σ -accuracies in the following sections.

2.3 Non-tidal loading data

The IERS 2010 conventions [Petit and Luzum, 2010] do not recommend the addition of NTL deformations in the calculation of the displacement of a reference point, as their modelling accuracy is low and their impact on the geodetic parameters compared to other deformations is small. However, their inclusion can be beneficial in geodetic analyses, as pointed out in recent studies [Glomsda et al., 2020; Singh et al., 2021], as the accuracy of the loading effect due to NTL has improved over the past years due to the improved accuracy of the numerical weather models used for its calculation [Jungclaus et al., 2013; Dill and Dobsław, 2013; Gelaro et al., 2017; Hersbach et al., 2018].

The IERS established the Global Geophysical Fluids Center (GGFC) in 1998, which has different bureaus responsible for research and data provision related to the redistribution of masses in atmosphere, oceans, and hydrological (land water) systems. The time series of NTLs over different time spans, based on calculations using numerical weather models and Green’s functions [Farrell, 1972; Dill and Dobsław, 2013; Petrov, 2015], can be obtained from these bureaus. These loadings can be added as observation level corrections in the calculation of the instantaneous position of a reference site.

In this study, we use the NTL provided by the International Mass Loading Service (IMLS)⁵. It provides three non-tidal loadings (atmosphere: NTAL, ocean: NTOL, and hydrological: HYDL), which occur due to redistribution of masses in atmosphere, oceans, and land water. For further details we refer the reader to our previous study [Singh et al., 2021], where we discussed the effect of NTL as observation level corrections in LUNAR, and gave the details of the differences of the NTL data from different data centres, described the different components of the NTLs, including discussions on specifics such as resolution, numerical weather models used for each loading, etc. Overall, from that study, we concluded that the addition of NTL in LUNAR, primarily from the IMLS, leads to small benefits in reduction of the weighted root mean square (WRMS) of LLR residuals, reduced the annual signal visible in the LLR residuals, and improved the estimation of station coordinates.

The loading deformation can be defined in a centre of figure (CF) frame (realised from the positions of geodetic stations on the solid Earth) or centre of mass (CM) frame (centre of orbiting satellites). This is controlled by the choice of degree-one load Love numbers, which enter the Green’s function summation [Petrov and Boy, 2004; Dill and Dobsław, 2013; Petrov, 2015] to calculate the effect of NTL. For further details on the differences between CM and CF, we refer to Sun [2017]. In our LLR analysis, the a-priori station positions are aligned to the CM frame and therefore the loadings used in this study were chosen in the CM frame.

3 Estimation of ΔUT

As mentioned in 2.2, the nights for which the ERP are estimated are categorised into different subsets. The ΔUT values were estimated for the nights of these subsets, using a-priori values from the combination of KEOF COMB2019 and IERS 14 C04 series, as described above. In the subsections that follow, we discuss the results of the estimated values of ΔUT and their accuracy, their correlations with various parameters, and the effect of NTL on ΔUT .

For the estimation of ΔUT , the velocities of the LLR observatories are fixed to ITRF 2014 solution values, and the values of the PMC (x_p and y_p) are fixed to their a-priori values.

3.1 Estimated values

For the estimation of ΔUT , the accuracy of the estimated values becomes better (i.e. smaller standard deviations) over the years. This is due to the improved accuracy of the NPs measured over the years, primarily due to the improved accuracy of the OCA green laser data, the highly accurate IR NP data (starting 2015), and the highly accurate APOLLO data (starting 2006). The differences of the estimated values from LUNAR to the values from IERS 14 C04 also become smaller over the time span, indicating the close agreement of the ΔUT values from the different space geodetic techniques (VLBI and LLR) with highly accurate data, thereby also validating each other.

Fig. 2 shows the accuracy of the ΔUT values for the subsets All05, All10, and All15, and Fig. 3 shows the accuracy of the ΔUT values for the subsets OCA05, OCA10, and OCA15. As the accuracy of the ΔUT values show a significant improvement in the recent years, we split the figure of each subset into two time spans, setting a break at 0h UTC 01.01.2000 (henceforth, ‘2000.0’). Additionally, Table 3 shows the mean values of all subsets considered in this study and the mean of the differences of the estimated values to the values of the IERS 14 C04 series. The values given in Table 3 are also split into two time spans, to show the differences in the estimation from the overall time span to the new data and to stress upon the best possible quality of the estimation from LLR.

The differences to the IERS 14 C04 series are primarily due to the different space geodetic techniques used to obtain the ΔUT values. Moreover, the C04 series is a combined product of different space geodetic techniques, and this combination also contributes to the improvement of the final product. As the results presented in this study are only from LLR analysis, a part of the differences could occur due to the difference in obtaining the final ΔUT values. A part of these differences are presumed to occur because of the different realisations of the International Celestial Reference System (ICRS) from VLBI and LLR. Additionally, they could be due to systematic errors in our calculation.

From Fig. 2, Fig. 3, and Table 3, it can be seen that the stricter the selection criteria, i.e. only those nights selected for ERP estimation with a higher number of NPs per night, the better the results. However, it must also be noted that the improvement in the results with the strict selection criteria is more stark in

⁵<http://massloading.net/>

the results until 2000.0, and leads to less improvement in the results after 2000.0, indicating that the very strict selection criteria is needed for data with low accuracy and that with the improvement of the accuracy of the NPs, a less strict selection criteria of the nights can be chosen. Additionally, it can be seen from Table 3 that the solution from the subsets of nights chosen from all observatories perform worse than the solution from the subsets of nights chosen from OCA only for the results before 2000.0. This is due to the reason that the accuracy of the NPs involved in the respective time spans of the subsets is significantly better from OCA compared to when NPs from all observatories are chosen. However, when considering the results of all solutions after 2000.0, the results from the solutions of the ‘All’ subsets perform better than those from the solutions of the ‘OCA’ subsets, as the accuracy of the NPs (in this time span) from all observatories is comparable and the solutions of ‘All’ subsets benefit from having more data and having a global coverage of the NPs involved and including the very good APOLLO data.

Using the radius of Earth (at the equator) as 6378 km, 10 μ s corresponds to 4.6 mm on the Earth’s radius, implying that the best possible (and current) accuracy of estimation of Δ UT (subset All15, after 2000.0) from LLR corresponds to a resolution of 7.3 mm on Earth’s surface. Compared to the resolution obtained from VLBI of 0.5 mm - 2.5 mm, LLR still lags behind VLBI, however its long time span and the possibility of dynamic realisation can be beneficial for some applications. Additionally, the results from LLR can be used to validate the results from VLBI.

Table 3: Mean values of the accuracy of Δ UT values obtained from different subsets (‘Mean 3σ ’ in table), and the mean of absolute changes to Δ UT values (i.e. differences of estimated values to the values from the IERS 14 C04 series (‘Mean diff.’ in table)) for the results from the beginning of any dataset until 2000.0 and the results after 2000.0.

Subset	Before 2000.0 [μ s]		After 2000.0 [μ s]	
	Mean 3σ	Mean diff.	Mean 3σ	Mean diff.
Apollo05	-	-	14.96	116.31
Apollo10	-	-	15.92	98.99
OCA05	96.31	204.35	30.71	69.07
OCA10	71.06	155.32	20.27	50.04
OCA15	53.56	128.89	16.53	39.95
All05	115.52	253.96	24.79	82.88
All10	74.13	169.21	18.63	56.91
All15	63.56	154.12	15.89	44.27

3.2 Correlations

The correlations of different parameters which are estimated in LUNAR with the ERP of the different estimated nights (henceforth, only ‘correlations’, in this section) were briefly discussed by Biskupek [2015]. In this study, as mentioned before, the velocities of the LLR observatories were kept fixed to the ITRF2014 solution values, as they have shown high correlations with the estimated ERP in previous studies.

One of the benefits of estimating the ERP from only one observatory (compared to estimating from all observatories) is that it leads to a reduction in the correlations estimated within LUNAR, as also visible by Table 4, where we show the value of the maximum correlation of Δ UT for any night with any non-ERP parameter, obtained from each subset.

Table 4: The maximum correlation of Δ UT of any night with any non-ERP estimated parameter, obtained from each subset.

Subset name prefix	Subset name suffix		
	05	10	15
Apollo	50 %	30 %	-
OCA	40 %	20 %	20 %
All	80 %	70 %	30 %

Overall, most parameters show no or very low correlation with the Δ UT values of any night. For the subsets from all observatories, the highest correlation, from all three subsets, of 80 %, 70 %, and 30 % is with the y-coordinate of WLRS. The parameters, from all three ‘All’ subsets, which show more than a 30 % correlation with the Δ UT values of any night are: the coordinates and/or biases of APOLLO, MLRS, LURE, OCA, and WLRS. Additionally, the x-coordinate of the L1 reflector shows a 30 % correlation only for the subset All05. For the subsets from OCA, the parameters (from all three OCA subsets) which show more than a 20 % correlation with the Δ UT values of any night are only the coordinates and biases of OCA. For the subsets from APOLLO, the parameters (from both APOLLO subsets) which show more than a 30 % correlation with the Δ UT values of any night are the coordinates and biases of APOLLO. Additionally, for the subset Apollo05, the x-coordinate of OCA and the x-coordinate of the L1 reflector shows a 30 % correlation.

Overall, the correlation between Δ UT values and the positions of LLR observatories is as expected. Additionally, the correlations with parameters such as the coordinates of lunar reflector disappear (or become smaller, and therefore irrelevant) when implementing the stricter selection criteria (10 or 15 NPs per night)

3.3 Effect of NTL on Δ UT

As there are correlations between the station coordinates and Δ UT, and as the addition of NTL leads to small benefits in our previous study, we decided to test the effect of including

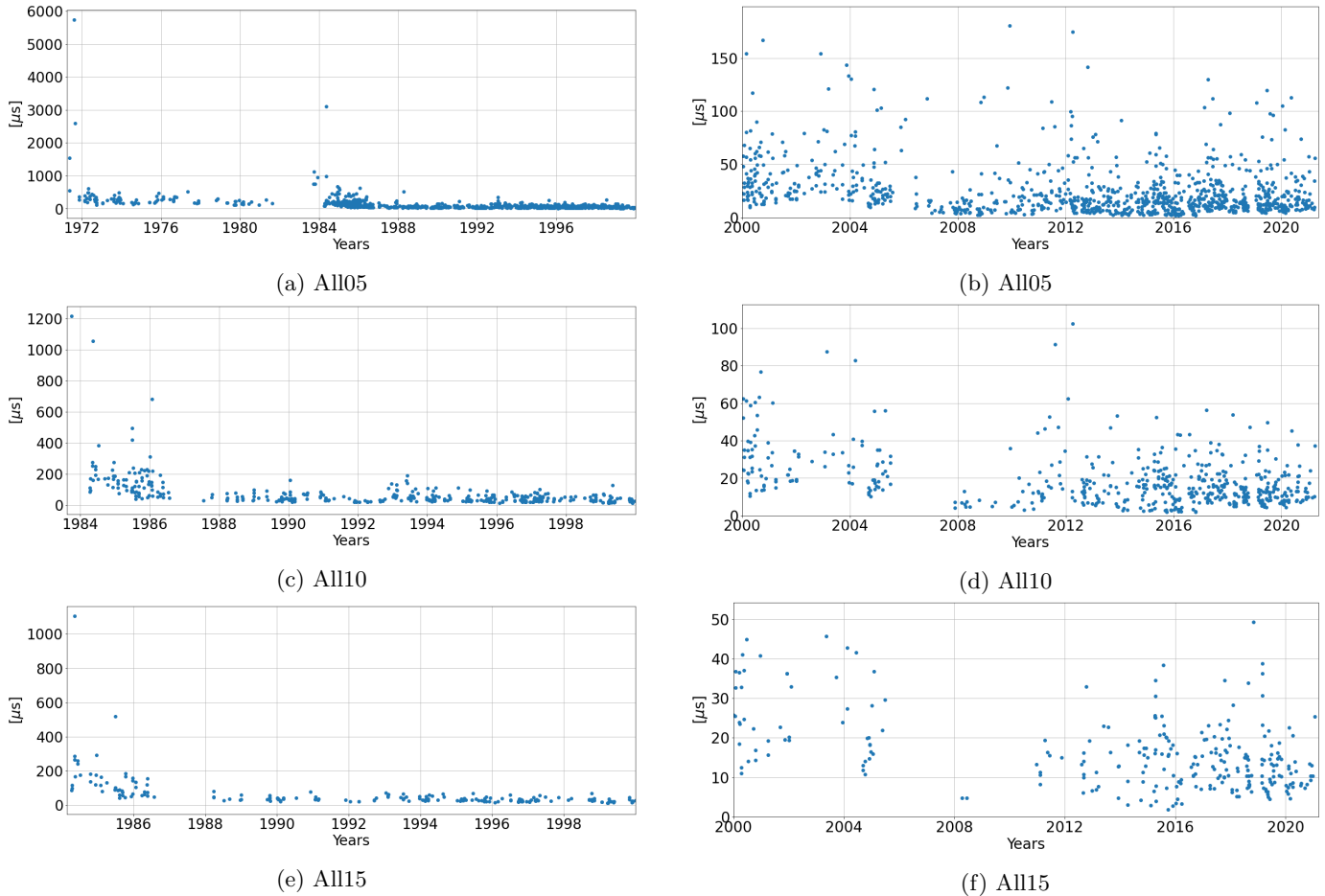


Figure 2: Accuracy of the estimated values of ΔUT for the subset All05, All10, and All15: in (a), (c), and (e) from the beginning of the dataset until 2000.0, and in (b), (d), and (f) from 2000.0 until the end of the dataset. Note the differences in the range of the axes for each sub-figure.

NTL in the ERP determination from LUNAR. Here, we added NTL only from IMLS, as it performed the best in LLR analysis [Singh et al., 2021]. We represent the combination of its three components (NTAL, NTOL, and HYDL) as NTSL. The effect of NTL, as expected, is of similar - small - magnitude on the estimated ΔUT values from all subsets for which the calculations were performed. In Fig. 4, we show the effect when adding NTSL to the standard solution for the estimation of ΔUT from the subset All15. Additionally, in Table 5, we show the mean values of the accuracy obtained for the estimation of ΔUT from the subsets All10 and All15 for the standard solution and the NTL solutions from IMLS. For the both the subsets, the NTSL solution improves the accuracy by 0.9%.

As the effect of adding NTL is similar for the whole time span, its effect on the results of the estimation of ΔUT does not change significantly when considering the entire time span of any subset, or only the time span which includes NPs with higher accuracy. Additionally, the inclusion of NTSL does not change the correlations, compared to the standard solution, at all. In Fig. 5, we show a comparison of the effect of NTSL on ΔUT values (absolute values) with the accuracies of the estimation of ΔUT values for the results after 2000.0 (for the subset All15), as the accuracies in this time span are significantly better than before 2000.0. It can be seen that both, the absolute

Table 5: Mean values of the accuracy of ΔUT for the standard and the NTL solutions for the subsets All10 and All15.

	Loading	All10 [μs]	All15 [μs]
Std		42.31	35.80
IMLS	NTAL	42.15	35.68
	NTOL	42.23	35.74
	HYDL	42.11	35.64
	NTSL	41.92	35.47

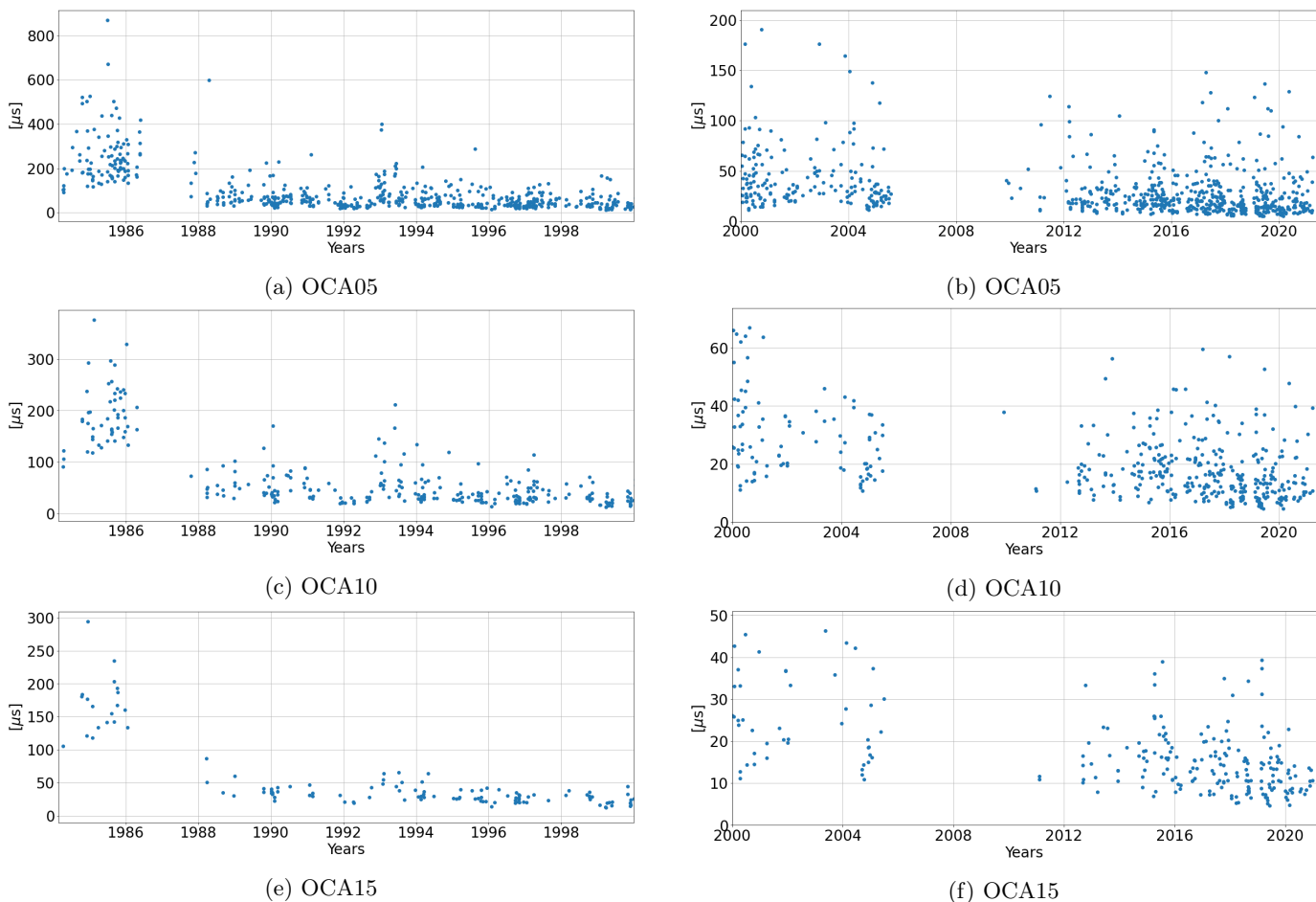


Figure 3: Accuracy of the estimated values of ΔUT for the subset OCA05, OCA10, and OCA15: in (a), (c), and (e) from the beginning of the dataset until 2000.0, and in (b), (d), and (f) from 2000.0 until the end of the dataset. Note the differences in the range of the axes for each sub-figure.

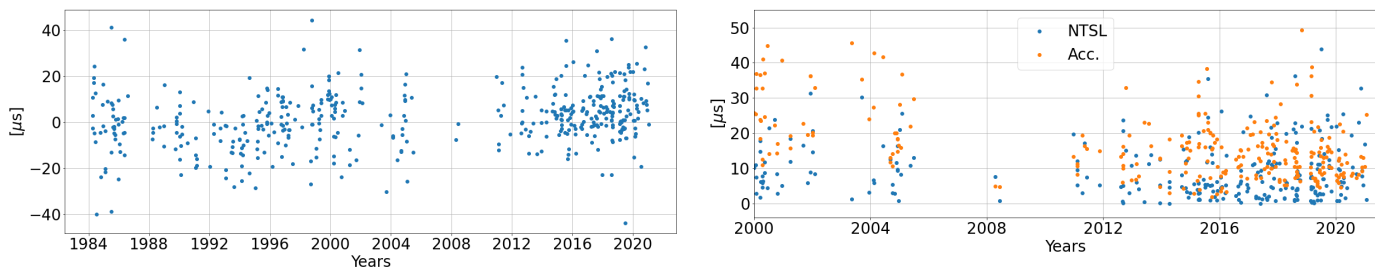


Figure 4: Estimated values of ΔUT for the NTSL solution from IMLS subtracted from the estimated values of the standard solution for the subset All15.

Figure 5: Absolute values of the effect when adding of NTSL on ΔUT values (in blue) and the accuracies of the estimated ΔUT values (in orange) for the subset All15, after 2000.0.

effect of NTSL on ΔUT and the accuracies of the ΔUT values, are in a similar range. For the subset All15, shown in Fig. 5, the mean of the effect of NTSL (absolute values) is $9.13 \mu s$, and the mean of the accuracy of ΔUT is $15.89 \mu s$ (see Table 3). Even though its effect is not significantly larger than accuracies obtained of ΔUT values, we assess that there is a small improvement in the overall accuracy of the estimated ΔUT values when including the NTSL. The improvement of the results due to the addition of IMLS NTSL is in sync with the findings from our previous study [Singh et al., 2021].

4 Estimation of terrestrial pole offsets

The PMC were estimated (for the nights of all subsets, Table 2), using a-priori values from the combination of KEOF COMB2019 and IERS 14 C04 series, as mentioned previously. In the subsections that follow, we discuss the results of the estimated values of x_p and y_p and their accuracy, their correlations

with each other and with other parameters, and the effect of NTL on them.

For the estimation of x_p and y_p , the velocities of the LLR observatories were fixed to the ITRF 2014 solution values, as it was also done for ΔUT estimation (see section 3), and the values of ΔUT were fixed to their a-priori values.

4.1 Estimated values

The estimation of x_p and y_p (following the GMM) gives the possibility of estimating x_p and y_p individually, or together. In the previous results of x_p and y_p estimation from LUNAR [Biskupek, 2015], the estimation was done individually, as the correlation between the x_p and y_p values (of the same night) is high, and the adjusted values were deemed to be more realistic when the adjustment was performed individually. With the expansion of the LLR dataset over the past years (providing a longer time series), more NPs recorded per night, and improved coverage of the lunar orbit mainly because of the benefits using IR laser pulses from OCA, the estimation of x_p and y_p together from has benefited. In this study, we estimate the PMC together and separately, for all subsets mentioned in Table 2, and compare the results. In Table 6, we give the mean values of the accuracy of x_p and y_p achieved, and the differences of the adjusted values to the IERS 14 C04 series. Additionally, as we did for ΔUT values, we split the results of PMC into two time spans, setting a break at 2000.0, for each subset, due to the stark improvement in the involved NPs and the results obtained over the LLR time span.

Fig. 6 shows the accuracy of the PMC values for the subsets All05, All10, and All15, also split into two time spans, with a break at 2000.0. Both, the figure and Table 6, give manifold results, discussed below.

As the x-axis for the polar motion is defined by the Greenwich meridian, and the the y-axis is defined by the line joining the 90° meridian (see Fig. 2 of Combrinck [2009]), OCA is (and other European observatories would be) more sensitive to the estimation of x_p compared to y_p , whereas APOLLO is (and other American observatories would be) more sensitive to the estimation of y_p compared to x_p . This can also be seen by Table 6, where the mean accuracy of the estimated x_p values is better than the mean of the estimated y_p values, for the results after 2000.0 (for the ‘OCA’ and ‘All’ subsets). This is, however, not visible for the results before 2000.0, probably because of the combination of the worse accuracy of the NPs involved along with the high sensitivity of OCA to the x-axis. The results of x_p show a higher improvement between the split subsets, compared to y_p (for example, mean values of x_p improves by 80.79 % from 9.42 mas to 1.81 mas for the subset OCA10, whereas the mean value of y_p improves by 70.89 % from 8.69 mas to 2.53 mas). As described in section 2.1, the LLR data is not evenly distributed with OCA contributing to over 60 % of the NPs, leading to better estimation of x_p from the subsets which consider NPs from all observatories as well, as most nights in the three subsets from all observatories are from OCA.

Other than to avoid high correlation between the estimated PMC of the same night, the individual estimation of x_p and y_p also helps see whether the estimation of both x_p and y_p is stable

or not. As seen in Table 6, the mean values of the accuracies of x_p and y_p change the most for the subsets made from selection of 5 NPs per night, and change the least for selection of 15 NPs per night, indicating that the calculations with selection of only 5 NPs per night are not as stable as those with a higher number of NPs selected per night. Additionally, it can be seen that the results for the subsets from APOLLO change drastically when estimating x_p and y_p individually, compared to their estimation together, even though the NPs from APOLLO are the most accurate, amongst all NPs. This indicates that the estimation of the PMC is more stable when the number of nights for which the estimation is performed is higher.

Table 6 also gives the differences obtained between the PMC values obtained from LUNAR and the IERS 14 C04 series. These differences follow the same trend as the accuracies, i.e. the results with the best accuracies have the least differences to the C04 series. These differences, as was also the case for differences of ΔUT from the C04 series, are presumed to be due to the different space geodetic techniques involved in formation and combination of the final product. Additionally, they could also be caused by some systematic errors in our calculation.

For the resolution of PMC, 1 mas corresponds to 3 cm on the Earth’s surface, implying that the current and best possible resolution of the PMC from LLR (subset All15, after 2000.0) is at 3.5 cm for x_p and at 4.6 cm for y_p on Earth’s surface. Compared to the resolution obtained from other space geodetic techniques, such as GNSS, the results of PMC estimation from LLR lag far behind.

4.2 Correlations

As mentioned before, when estimating the PMC together, the values of x_p and y_p in the same night are correlated to each other. These correlations can be as high as 100 %, indicating advantage of estimating the PMC separately. In Fig. 7, we give the correlation of the x_p and y_p estimated in the same night with each other, from the subsets OCA05, OCA10, and OCA15. The trend followed by the other subsets is the same, i.e., the correlations of the subsets chosen with 5 NPs per night are the highest, with the PMC of many nights showing a 100 % correlation with each other. With the selection of 15 NPs per night, none of the nights (for OCA15) show a correlation of 100 % with each other, further proving the benefit of the strict selection criteria of subsets for ERP estimation from LLR. However, even with 15 NPs per night, the correlations of the x_p and y_p estimated in the same night with each other are very high.

For the correlation of the estimated x_p and y_p with the non-ERP parameters of LUNAR, the trend followed is the same as that for the estimation of ΔUT values, i.e., the correlation of the estimation from ‘All’ subsets is higher than the correlation of the estimation of ERP from nights selected from any one observatory. In Table 7, we show the value of the maximum correlations of x_p and y_p of any night with any non-ERP parameter for each subset.

As it was the case with correlations of ΔUT with non-ERP parameters, most parameters show either no or very low correlation with the estimated x_p and y_p . The parameters which show the maximum correlations, whether the PMC are estimated to-

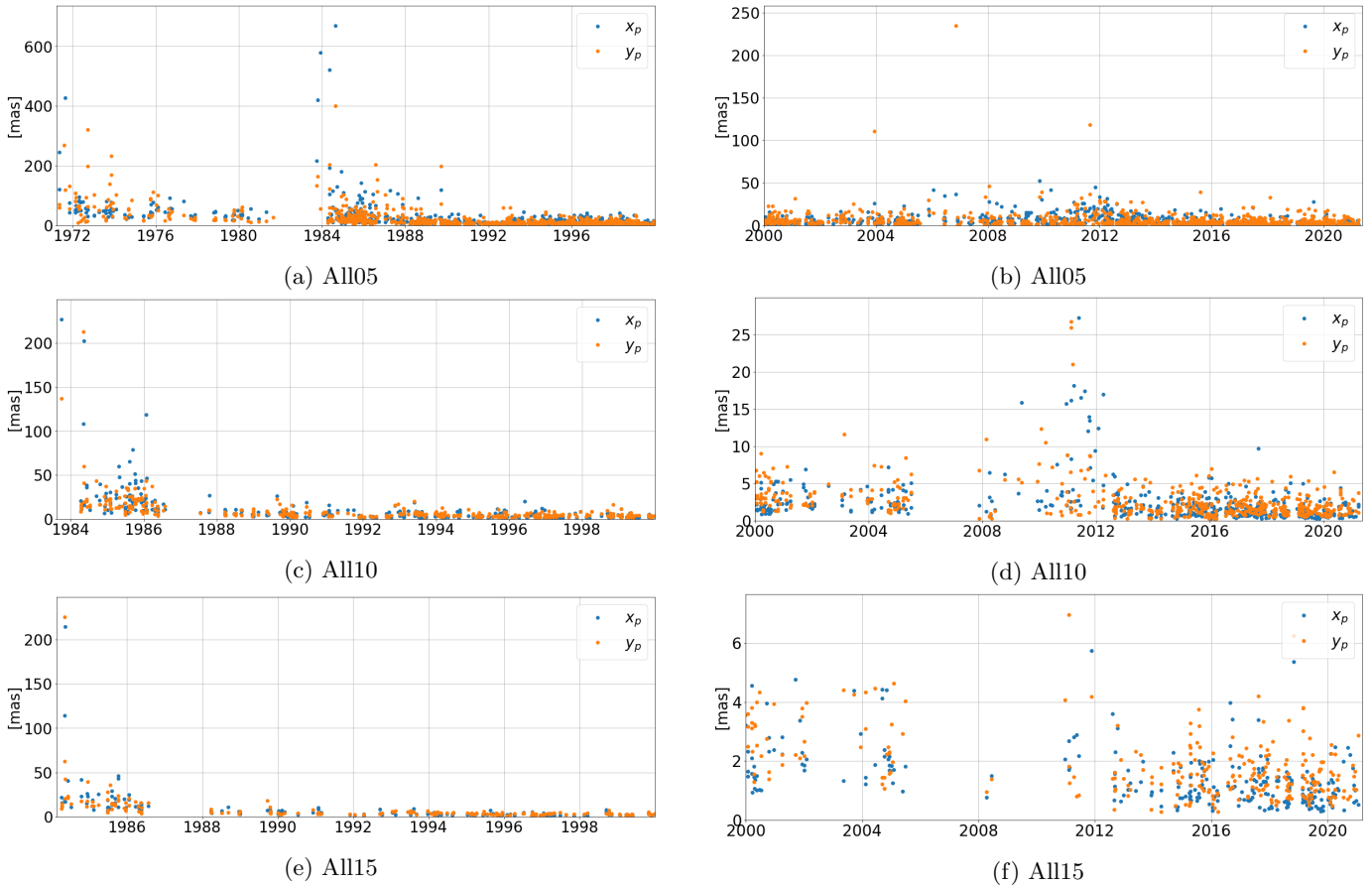


Figure 6: Accuracy of the estimated values of PMC for the subset All05, All10, and All15: in (a), (c), and (e) from the beginning of the dataset until 2000.0, and in (b), (d), and (f) from 2000.0 until the end of the dataset. Note the differences in the range of the axes for each sub-figure.

gether or separately, stay the same. The highest correlations from the subset All05 and All10 are with the position of MAUI and MLRS. For the subset All15, the highest correlations are with the position of WLRs. Overall, the parameters which show a 40% correlation or more with either x_p and y_p are the station coordinates and/or biases of the LLR observatories. For OCA05 and OCA10 subsets, the highest correlation reach up to 50%, where, 30% or higher correlation is achieved only by the coordinates and/or biases of OCA. For Apollo05, the maximum correlations reach up to 60%, where the parameters which show a 30% or higher correlation are only the coordinates and/or biases of APOLLO. For Apollo10, only the coordinates and/or biases of APOLLO show a 20% or more correlation, reaching a maximum of 40%.

The parameters which show a correlation with the PMC are the same, whether the estimation is done separately or together. The percentage by which they are correlated also stays very similar, as can also be seen in Table 7 (specially for the subsets with the strict selection criteria of 15 NPs per night). The difference in correlations between these two cases is that more nights show a correlation with those parameters when the estimation of PMC is done separately. Some effect is also absorbed by the correlation between the x_p and the y_p of the same night.

4.3 PMC signal analysis

The polar motion has three major components: Chandler wobble, annual oscillation, and a drift along the 80° West meridian. When applying a Fourier transformation of the PMC from the IERS 14 C04 series (not shown), signals with an annual period and a Chandler period are visible. As the LLR NPs are temporally unevenly distributed, a Fourier transformation of the estimated PMC values is not possible. To perform a spectral analysis of a non-uniformly distributed data, we used the Lomb-Scargle (LS) periodogram. However, to obtain a very clear distribution, a high sampling rate and uniformity of data samples is beneficial [VanderPlas, 2017], which is not given in LLR dataset. Due to these reasons, the LS power (not shown) at the annual and Chandler frequency component did not show similar high peaks as the Fourier transformation of the PMC from the IERS 14 C04 series for all subsets. In the difference of the powers obtained from the LS periodograms of the a-priori PMC values and the estimated PMC values from LUNAR, no change of the signals was visible when estimating PMC (whether together or separately).

Table 6: Mean values of the accuracies of the x_p and y_p values obtained from different subsets (3σ in table), and the mean of absolute changes to x_p and y_p values (i.e. differences of estimated values to the values from the IERS 14 C04 series ($Diff.$ in table)) for the results from the beginning of the dataset until 2000.0 in (a) and from 2000.0 until the end of the dataset in (b).

(a) Before 2000.0								
Subset	x_p and y_p [mas]				Only x_p [mas]		Only y_p [mas]	
	3σ		Diff.		3σ	Diff.	3σ	Diff.
	x_p	y_p	x_p	y_p	x_p	x_p	y_p	y_p
Apollo05	-	-	-	-	-	-	-	-
Apollo10	-	-	-	-	-	-	-	-
OCA05	13.79	13.68	3.75	4.07	9.91	3.26	9.63	3.29
OCA10	9.42	8.69	2.62	2.41	7.89	2.73	7.19	2.52
OCA15	7.39	5.95	2.55	2.16	6.75	2.54	5.29	2.16
All05	19.92	18.56	10.33	8.85	13.17	6.22	12.60	5.81
All10	9.66	8.73	2.93	2.65	8.10	3.06	6.96	2.48
All15	8.57	8.06	2.76	2.82	7.20	2.23	6.51	2.29
(b) After 2000.0								
Subset	x_p and y_p [mas]				Only x_p [mas]		Only y_p [mas]	
	3σ		Diff.		3σ	Diff.	3σ	Diff.
	x_p	y_p	x_p	y_p	x_p	x_p	y_p	y_p
Apollo05	8.41	6.88	9.13	5.89	2.22	2.64	1.48	1.63
Apollo10	5.89	4.55	3.85	2.61	2.19	2.40	1.31	1.37
OCA05	3.42	5.08	1.44	1.73	1.97	0.96	2.97	1.11
OCA10	1.81	2.53	0.78	0.68	1.38	0.79	1.97	0.78
OCA15	1.39	1.85	0.74	0.56	1.20	0.76	1.62	0.70
All05	4.49	5.37	3.25	2.87	1.99	1.37	2.59	1.28
All10	2.18	2.54	1.19	0.89	1.38	0.99	1.74	0.83
All15	1.38	1.77	0.81	0.59	1.16	0.83	1.52	0.73

4.4 Effect of NTL on estimated values

As the station coordinates and PMC are also correlated, we checked the effect when adding NTL for the estimation of PMC from LUNAR, as we did for ΔUT estimation. The NTL was added only from IMLS, in three individual loading components: NTAL, NTOL, and HYDL, and a fourth component of their combination: NTSL. The effect of NTL, as expected, is of similar - small - magnitude on the estimated PMC values from all subsets. In Fig. 8, we show the effect when adding NTSL to the standard solution for the estimation of PMC from the subset All15. Additionally, in Table 8, we show the mean values of the accuracy obtained for the estimation of PMC from the subsets All10 and All15 for the standard solution and the NTL

solutions from IMLS.

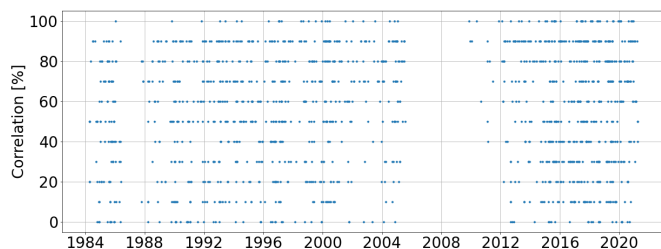
When adding NTL from any loadings, there was no change observed in the correlations of the PMC with the non-ERP parameters of LUNAR. In our previous study [Singh et al., 2021], we discussed the benefit of reduction of the annual signal in LLR residuals when adding NTL. However, as the data from the subsets is temporally extremely unevenly distributed, any effect the addition of NTL might have at the annual signal is masked by noise.

In Fig. 9, we show a comparison of the effect of NTSL on the PMC (absolute values) with the accuracies of the estimation of x_p and y_p values for the results after 2000.0 for the subset All15, as the best accuracies are obtained in this time span.

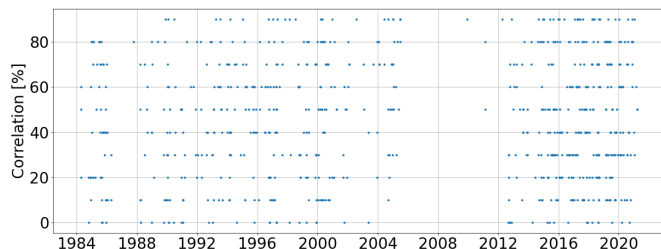
Table 7: The maximum correlations of x_p and y_p of any night with any non-ERP estimated parameter, obtained from each subset.

(a) x_p , estimation of PMC together				(b) y_p , estimation of PMC together			
Subset name prefix	Subset name suffix			Subset name prefix	Subset name suffix		
	05	10	15		05	10	15
Apollo	60 %	40 %	-	Apollo	60 %	30 %	-
OCA	50 %	30 %	30 %	OCA	30 %	20 %	10 %
All	100 %	100 %	40 %	All	90 %	90 %	30 %

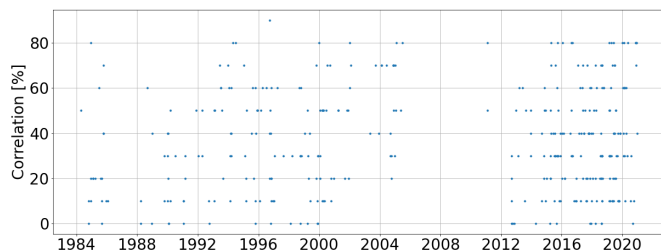
(c) x_p , estimation of only x_p				(d) y_p , estimation of only y_p			
Subset name prefix	Subset name suffix			Subset name prefix	Subset name suffix		
	05	10	15		05	10	15
Apollo	50 %	30 %	-	Apollo	60 %	30 %	-
OCA	50 %	30 %	30 %	OCA	40 %	20 %	10 %
All	80 %	80 %	40 %	All	70 %	60 %	40 %



(a) OCA05



(b) OCA10



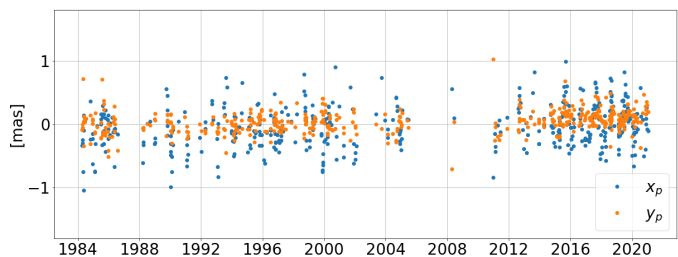
(c) OCA15

 Figure 7: Correlation of x_p and y_p estimated in the same night with each other, from the subsets OCA05, OCA10, and OCA15.

It can be seen that the absolute effect of NTSL is significantly smaller than the accuracies of the x_p and y_p values. In spite

Table 8: Mean values of accuracy of the PMC values for the standard and the NTL solutions for the subsets All10 and All15.

	Loading	All10 [mas]		All15 [mas]	
		xp	yp	xp	yp
Std		5.37	5.18	4.36	4.40
IMLS	NTAL	5.34	5.15	4.34	4.37
	NTOL	5.35	5.17	4.35	4.38
	HYDL	5.35	5.16	4.35	4.39
	NTSL	5.31	5.13	4.32	4.35


 Figure 8: Estimated values of x_p and y_p for NTSL solution from IMLS subtracted from the estimated values of the standard solution for the subset All15.

of the effect being smaller, there is a small improvement in the overall accuracy of the estimated ΔUT values when including the NTSL, see Table 8. Overall, the accuracy of the PMC improves for the IMLS NTSL solutions (about 1% for both components of both subsets). As mentioned previously, these changes are in sync with the findings from our previous study [Singh et al., 2021].

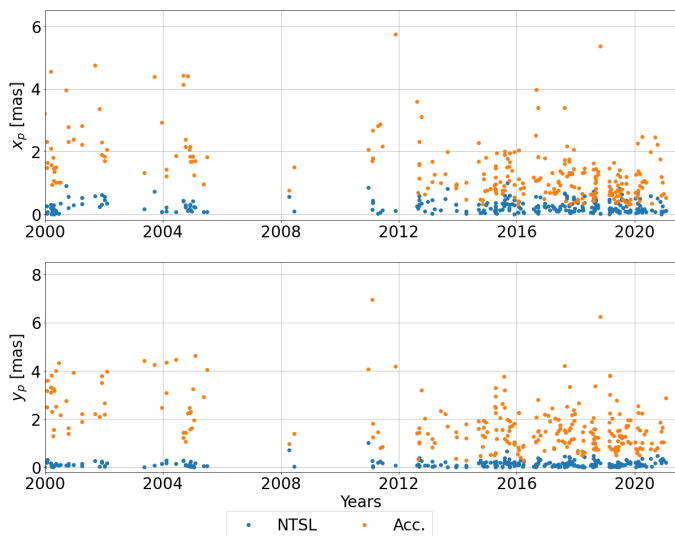


Figure 9: Absolute values of the effect of addition of NTSL on x_p and y_p and the values of accuracies for the estimated x_p and y_p for the subset All15, after 2000.0.

5 Conclusions

In this study, we estimated the Earth rotation parameters, Earth rotation phase, ΔUT , and the terrestrial pole offsets, x_p and y_p , from LLR analysis for eight different subsets of nights in the LLR time span. We estimated the ERP by performing a least square adjustment using the Gauss-Markov model. For the analysis, we kept the velocities of the LLR observatories fixed to the ITRF2014 solution values, and estimated ΔUT and the PMC separately, to avoid high correlations between them. For the estimation of PMC, we estimated x_p and y_p together and separately. We discussed the differences of the estimated ERP results to the IERS 14 C04 series, for the different subsets, analysed the accuracy of their estimation, and additionally discussed the effect of addition of NTL on the ERP estimation.

Generally, the estimation of ERP shows a significant improvement over the time span of the subsets considered in this study, with the mean accuracy of the estimated values reducing to (almost) a third of its value when comparing the results split at 0h UTC 01.01.2000. The best possible resolution of estimated ERP (on Earth's surface) is of 7.3 mm (i.e. 15.89 μs) from ΔUT estimation, and of about 4 cm from the estimation of PMC (i.e. 1.16 mas for x_p and 1.52 mas for y_p). Compared to other space geodetic techniques, the results from LLR still lag behind, however are still important, as LLR provides the longest time series of any space geodetic technique and is the only technique other than VLBI which provides ΔUT values. With the more accurate and more frequent LLR data in future, possibly with the measurements using differential LLR [Viswanathan et al., 2021], better results for ERP can be expected from LLR.

LLR is more sensitive to the estimation of ΔUT values than PMC values. This is due to low number of NPs per night used within the estimation, combined with the fact that changes per night are larger for ΔUT than for the PMC. Furthermore, due to the distribution of the LLR data (most NPs are measured from OCA), the estimation of PMC from LLR is more sensitive to x-

direction than to y-direction. The values of the mean accuracy obtained from different subsets, shown in Table 6, where the values of x_p are smaller than y_p , and the improvement in the values of x_p is more significant than in y_p , when comparing the results from the old NPs (before 2000.0) to the results from the new NPs (after 2000.0).

For the estimation of PMC, with the estimation of x_p and y_p together and separately, we were able to assess the stability of the calculation. With the subsets which were selected with a strict selection criteria of either 10 or 15 NPs per night, and when the number of estimated nights was not too few (such as for the subset Apollo10, 63 nights) the results of the estimated x_p and y_p values were not too different from each other when estimated individually or together.

The estimated ERP are primarily correlated to the positions of the observatory the nights were selected from. With a more strict selection criteria (15 NPs per night instead of 5 NPs per night), the correlations reduce significantly, however, this comes at the cost of having fewer nights at which the ERP can be estimated. The estimated PMC (when estimated together) are highly correlated to each other (x_p and the y_p values of the same night), with correlations going as high as 100%. These correlations come down to a highest of 80% with the strict selection criteria of 15NPs per night from one observatory, however are still too high. With the less strict selection criteria of 5 NPs per night, the ERP show correlations up to 20% and 30% with some parameters such as reflectors, the rotational time lags of the Earth (diurnal and semi-diurnal, due to the tidal effect of the Moon), etc., which disappear (or become smaller, and therefore irrelevant) when implementing the stricter selection criteria.

The NTL was applied as observation level corrections in our LLR analysis and added as three different loading constituents for mass redistribution in atmosphere, oceans, and land water from the IMLS dataset. The impact when adding all three components of NTL on ERP estimation is smaller in magnitude than the accuracies of the ERP values, for both ΔUT and PMC. However, it leads to about 1% improvement in the accuracies obtained, and is therefore recommended to be added for ERP estimation.

Acknowledgements

We acknowledge with thanks that the processed LLR data, since 1969, has been obtained under the efforts of the personnel at the Observatoire de la Côte d'Azur in France, the LURE Observatory in Maui, Hawaii, the McDonald Observatory in Texas, the Apache Point Observatory in New Mexico, the Matera Laser Ranging observatory in Italy, and the Wettzell Laser Ranging System in Germany. This research was funded by the German Aerospace Center's (DLR) Institute for Satellite Geodesy and Inertial Sensing, and Deutsche Forschungsgemeinschaft (DFG, German Research Foundation) under Germany's Excellence Strategy EXC 2123 QuantumFrontiers, Project-ID 390837967. We would additionally like to thank Franz Hofmann for his contributions to LUNAR.

Data availability

LLR data is collected, archived, and distributed under the auspices of the International Laser Ranging Service (ILRS) [Pearlman et al., 2019]; and downloaded from the website⁶. The IMLS non-tidal loading dataset is freely available on the IMLS website⁷; and downloaded for the LLR observatories from the pre-computed time series of 1272 space geodesy sites. The KEOF COMB2019 EOP time series is freely available at the website⁸, and the IERS 14 C04 EOP time series is freely available at the website⁹.

Author contributions

All authors contributed to the development of this study and provided ideas to its content. Data collection and analysis were performed by VVS, LB, and MZ. The first draft of the manuscript was written by VVS, and all authors commented on previous versions of the manuscript. All authors read and approved the final manuscript.

References

- R. Bauer. *Bestimmung von Parametern des Erde-Mond-Systems - Ein Beitrag zur Modellerweiterung und Bewertung, Ergebnisse* -. PhD thesis, Technische Universität München, 1989. Deutsche Geodätische Kommission bei der Bayerischen Akademie der Wissenschaften, Reihe C, Nr. 353.
- L. Biskupek. *Bestimmung der Erdorientierung mit Lunar Laser Ranging*. PhD thesis, Leibniz University Hannover, Deutsche Geodätische Kommission bei der Bayerischen Akademie der Wissenschaften, Reihe C, Nr. 742, 2015. doi: 10.15488/4721.
- L. Biskupek, J. Müller, and J.-M. Torre. Benefit of new high-precision llr data for the determination of relativistic parameters. *Universe*, 7(2), 2021. doi: 10.3390/universe7020034.
- C. Bizouard, S. Lambert, C. Gattano, O. Becker, and J.-Y. Richard. The IERS EOP 14C04 solution for Earth orientation parameters consistent with ITRF 2014. *Journal of Geodesy*, 93(5):621–633, 2019. doi: 10.1007/s00190-018-1186-3.
- N. Capitaine. The Determination of Earth Orientation by VLBI and GNSS: Principles and Results. In E. F. Arias, L. Combrinck, P. Gabor, C. Hohenkerk, and P. K. Seidelmann, editors, *The Science of Time 2016*, pages 167–196, Cham, 2017. Springer International Publishing.
- J. Chabé, C. Courde, J.-M. Torre, S. Bouquillon, A. Bourgoïn, M. Aïmar, D. Albanèse, B. Chauvineau, H. Mariey, G. Martinot-Lagarde, N. Maurice, D.-H. Phung, E. Samain, and H. Viot. Recent Progress in Lunar Laser Ranging at Grasse Laser Ranging Station. *Earth and Space Science*, 7: e2019EA000785, 2020. doi: 10.1029/2019EA000785.
- W. Combrinck. Products of Space Geodesy and Links to Earth Science and Astronomy. 2009. ISSN 2214-4609. doi: 10.3997/2214-4609-pdb.241.combrinck_wl_paper1. Conference Proceedings, 11th SAGA Biennial Technical Meeting and Exhibition, cp-241-00039 .
- J. O. Dickey, X. X. Newhall, and J. G. Williams. Earth Orientation From Lunar Laser Ranging and an Error Analysis of Polar Motion Services. *Journal of Geophysical Research*, 90, 10 1985. doi: 10.1029/JB090iB11p09353.
- R. Dill and H. Dobsław. Numerical simulations of global-scale high-resolution hydrological crustal deformations. *Journal of Geophysical Research: Solid Earth*, 118(9):5008–5017, 2013. doi: 10.1002/jgrb.50353.
- D. Egger. *Systemanalyse der Laserentfernungsmessung*. PhD thesis, Technische Universität München, 1985. Deutsche Geodätische Kommission bei der Bayerischen Akademie der Wissenschaften, Reihe C, Nr. 311.
- W. E. Farrell. Deformation of the Earth by surface loads. *Rev. Geophys. and Spac. Phys.*, 10(3):751–797, 1972. doi: 10.1029/RG010i003p00761.
- W. M. Folkner, J. G. Williams, D. H. Boggs, R. S. Park, and P. Kuchynka. The Planetary and Lunar Ephemerides DE430 and DE431. *IPN Progress Report 42-196*, 2014.
- R. Gelaro, W. McCarty, M. J. Suárez, R. Todling, A. Molod, L. Takacs, C. A. Randles, A. Darmenov, M. G. Bosilovich, R. Reichle, K. Wargan, L. Coy, R. Cullather, C. Draper, S. Akella, V. Buchard, A. Conaty, A. M. da Silva, W. Gu, G.-K. Kim, R. Koster, R. Lucchesi, D. Merkova, J. E. Nielsen, G. Partyka, S. Pawson, W. Putman, M. Rienecker, S. D. Schubert, M. Sienkiewicz, and B. Zhao. The Modern-Era Retrospective Analysis for Research and Applications, Version 2 (MERRA-2). *Journal of Climate - American Meteorological Society*, 30(14):5419–5454, 2017. doi: 10.1175/JCLI-D-16-0758.1.
- H. Gleixner. *Ein Beitrag zur Ephemeridenrechnung und Parameterschätzung im Erde-Mond-System*. PhD thesis, Technische Universität München, 1986. Deutsche Geodätische Kommission bei der Bayerischen Akademie der Wissenschaften, Reihe C, Nr. 319.
- M. Glomsda, M. Bloßfeld, M. Seitz, and F. Seitz. Benefits of non-tidal loading applied at distinct levels in VLBI analysis. *Journal of Geodesy*, 94(90):1–19, 2020. doi: 10.1007/s00190-020-01418-z.
- H. HERSBACH, P. de Rosnay, B. Bell, D. Schepers, A. Simmons, C. Soci, S. Abdalla, M. A. Balmaseda, G. Balsamo, P. Bechtold, P. Berrisford, J. Bidlot, E. de Boissésou, M. Bonavita, P. Browne, R. Buizza, P. Dahlgren, D. Dee, R. Dragani, M. Diamantakis, J. Flemming, R. Forbes, A. Geer, T. Haiden, E. Hólm, L. Haimberger, R. Hogan, A. Horányi, M. Janisková, P. Laloyaux, P. Lopez, J. Muñoz-Sabater, C. Peubey, R. Radu, D. Richardson, J.-N. Thépaut, F. Vitart, X. Yang, E. Zsótér, and H. Zuo. Operational global reanalysis: progress, future directions and synergies with

⁶https://cddis.nasa.gov/About/CDDIS_File_Download_Documentation.html

⁷<http://massloading.net/>

⁸<https://keof.jpl.nasa.gov/combinations/latest/>

⁹<https://www.iers.org/IERS/EN/DataProducts/EarthOrientationData/eop.html;jsessionid=4593E0A857CFBA2E4141374D13DA2F55.live2>

- NWP. Technical Report 27, European Centre for Medium Range Weather Forecasts, Shinfield Park, Reading, Berkshire RG2 9AX, England, 2018.
- F. Hofmann. *Lunar Laser Ranging – verbesserte Modellierung der Mondodynamik und Schätzung relativistischer Parameter*. PhD thesis, Leibniz University Hannover, Deutsche Geodätische Kommission bei der Bayerischen Akademie der Wissenschaften, Reihe C, Nr. 797, 2017.
- F. Hofmann and J. Müller. Relativistic Tests with Lunar Laser Ranging. *Classical and Quantum Gravity*, 35-035015 (3), 2018. doi: 10.1088/1361-6382/aa8f7a.
- F. Hofmann, L. Biskupek, and J. Müller. Contributions to reference systems from Lunar Laser Ranging using the IFE analysis model. *Journal of Geodesy*, 92:975–987, 2018. doi: 10.1007/s00190-018-1109-3.
- J. H. Jungclaus, N. Fischer, H. Haak, K. Lohmann, J. Marotzke, D. Matei, U. Mikolajewicz, D. Notz, and J. S. von Storch. Characteristics of the ocean simulations in the Max Planck Institute Ocean Model (MPIOM) the ocean component of the MPI-Earth system model. *Journal of Advances in Modeling Earth Systems*, 5(2):422–446, 2013. doi: 10.1002/jame.20023.
- S. Kopeikin, E. Pavlis, D. Pavlis, V. Brumberg, A. Escapa, J. Getino, A. Gusev, J. Müller, W.-T. Ni, and N. Petrova. Prospects in the orbital and rotational dynamics of the Moon with the advent of sub-centimeter lunar laser ranging. *Advances in Space Research*, 42(8):1378–1390, 2008. ISSN 0273-1177. doi: 10.1016/j.asr.2008.02.014.
- J. Müller. *Analyse von Lasermessungen zum Mond im Rahmen einer post-Newton’schen Theorie*. PhD thesis, Technische Universität München, 1991. Deutsche Geodätische Kommission bei der Bayerischen Akademie der Wissenschaften, Reihe C, Nr. 383.
- J. Müller, L. Biskupek, J. Oberst, and U. Schreiber. Contribution of Lunar Laser Ranging to Realise Geodetic Reference Systems. In *Geodetic Reference Frames. International Association of Geodesy Symposia*, volume 134, pages 55–59. Springer Berlin Heidelberg, Berlin, Heidelberg, 10 2009. doi: 10.1007/978-3-642-00860-3-8.
- J. Müller, F. Hofmann, and L. Biskupek. Testing various facets of the equivalence principle using lunar laser ranging. *Classical and Quantum Gravity*, 29:184006, 09 2012. doi: 10.1088/0264-9381/29/18/184006.
- J. Müller, L. Biskupek, F. Hofmann, and E. Mai. Lunar laser ranging and relativity. In S. M. Kopeikin, editor, *Frontiers in relativistic celestial Mechanics*, volume 2: Applications and Experiments, pages 103–156. Walter de Gruyter, Berlin, 2014.
- J. Müller, T. W. Murphy, U. Schreiber, P. J. Shelus, J. M. Torre, J. G. Williams, D. H. Boggs, S. Bouquillon, A. Bourgoin, and F. Hofmann. Lunar Laser Ranging: a tool for general relativity, lunar geophysics and Earth science. *Journal of Geodesy*, 93:2195–2210, 2019. doi: 10.1007/s00190-019-01296-0.
- T. W. Murphy. Lunar laser ranging: the millimeter challenge. *Reports on Progress in Physics*, 76:076901, 2013. doi: 10.1088/0034-4885/76/7/076901.
- D. A. Pavlov, J. G. Williams, and V. V. Suvorkin. Determining parameters of Moon’s orbital and rotational motion from LLR observations using GRAIL and IERS-recommended models. *Celestial Mechanics and Dynamical Astronomy*, 126: 61–88, 2016. doi: 10.1007/s10569-016-9712-1.
- M. R. Pearlman, C. E. Noll, E. C. Pavlis, F. G. Lemoine, L. Combrink, J. J. Degnan, G. Kirchner, and U. Schreiber. The ILRS: approaching 20 years and planning for the future. *Journal of Geodesy*, 93(11):2161–2180, Nov. 2019. doi: 10.1007/s00190-019-01241-1.
- G. Petit and B. Luzum, editors. *IERS Conventions 2010*. Number 36 in IERS Technical Note. Verlag des Bundesamtes für Kartographie und Geodäsie, Frankfurt am Main, 2010.
- L. Petrov. The International Mass Loading Service, 2015. <http://arxiv.org/abs/1503.00191>.
- L. Petrov and J.-P. Boy. Study of the atmospheric pressure loading signal in very long baseline interferometry observations. *Journal of Geophysical Research: Solid Earth*, 109(B3), 2004. ISSN 148-227. doi: 10.1029/2003JB002500.
- J. T. Ratcliff and R. S. Gross. Combinations of Earth Orientation Measurements: SPACE2019, COMB2019, and POLE2019. Technical Report JPL Publication 20-3, Jet Propulsion Laboratory, 2020.
- H. Schuh and D. Behrend. VLBI: A fascinating technique for geodesy and astrometry. *Journal of Geodynamics*, 61:68–80, 2012. ISSN 0264-3707. doi: 10.1016/j.jog.2012.07.007.
- C. Sciarretta, V. Luceri, E. Pavlis, and G. Bianco. The ILRS EOP time series. *Artificial Satellites*, 45:41–48, 01 2010. doi: 10.2478/v10018-010-0004-9.
- V. V. Singh, L. Biskupek, J. Müller, and M. Zhang. Impact of non-tidal station loading in LLR. *Advances in Space Research*, 67(12):3925–3941, 2021. ISSN 0273-1177. doi: 10.1016/j.asr.2021.03.018.
- Y. Sun. *Estimating geocenter motion and changes in the Earth’s dynamic oblateness from GRACE and geophysical models*. PhD thesis, TU Delft Physical and Space Geodesy, 2017. doi: 10.4233/uuid:7fe64dde-7fb5-4392-8160-da6f7916dc6b.
- J. T. VanderPlas. Understanding the Lomb-Scargle Periodogram. *The Astrophysical Journal Supplement Series*, 236 (1):16, 2017. doi: 10.3847/1538-4365/aab766.
- V. Viswanathan, N. Rambaux, A. F. and J. Laskar, and M. Gastineau. Observational Constraint on the Radius and Oblateness of the Lunar Core-Mantle Boundary. *Geophysical Research Letters*, 46:7295–7303, 2019. doi: 10.1029/2019GL082677.
- V. Viswanathan, E. Mazarico, S. Merkowitz, J. Williams, S. Turyshev, D. Currie, A. Ermakov, N. Rambaux, A. Fienga, C. Courde, J. Chabé, J.-M. Torre, A. Bourgoin, K. Schreiber, M. Eubanks, C. Wu, D. Dequal, S. Dell’Agnello, L. Biskupek, J. Müller, and S. Kopeikin. Extending Science from Lunar Laser Ranging. *Bulletin of the American Astronomical Society*, 53, 03 2021. doi: 10.3847/25c2cfef.3dc2e5e4.

- J. G. Williams, S. G. Turyshev, D. H. Boggs, and J. T. Ratcliff. Lunar laser ranging science: Gravitational physics and lunar interior and geodesy. *Advances in Space Research*, 37:67–71, 2006. doi: 10.1016/j.asr.2005.05.013.
- J. G. Williams, S. G. Turyshev, and D. H. Boggs. Lunar Laser Ranging Tests of the Equivalence Principle with the Earth and Moon. *International Journal of Modern Physics D*, 18(7):1129–1175, 2009. doi: 10.1142/S021827180901500X.
- J. G. Williams, D. H. Boggs, and W. M. Folkner. DE430 Lunar Orbit, Physical Librations, and Surface Coordinates. Technical report, Jet Propulsion Laboratory, California Institute of Technology, Pasadena, CA, USA, 7 2013. Interoffice memorandum, IOM 335-JW,DB,WF-20130722-016.
- R. Zajdel, K. Sośnica, G. Bury, R. Dach, and L. Prange. System-specific systematic errors in earth rotation parameters derived from gps, glonass, and galileo. *GPS Solutions*, 24, 05 2020. doi: 10.1007/s10291-020-00989-w.
- W. Zerhouni and N. Capitaine. Celestial pole offsets from lunar laser ranging and comparison with VLBI. *Astronomy & Astrophysics*, 507:1687–1695, 12 2009. doi: 10.1051/0004-6361/200912644.
- M. Zhang, J. Müller, and L. Biskupek. Test of the equivalence principle for galaxy’s dark matter by lunar laser ranging. *Celestial Mechanics and Dynamical Astronomy*, 132(4): 25, 2020. ISSN 1572-9478. doi: 10.1007/s10569-020-09964-6.